

Article

Optimizing Non-Glare Zone Width of Adaptive Driving Beam (ADB) Using Fuzzy Logic Control

Yihong Chen ¹, Arash Ahmadi ² and Mohammed Jalal Ahamed ^{1,*} 

¹ Mechanical, Automotive and Materials Engineering, University of Windsor, Windsor, ON N9B 3P4, Canada; chen17t@uwindsor.ca

² Electrical and Computer Engineering, University of Windsor, Windsor, ON N9B 3P4, Canada; arash.ahmadi@uwindsor.ca

* Correspondence: jahamed@uwindsor.ca

Abstract: Adaptive driving beam (ADB) is an advanced vehicle forward-lighting system that automatically adapts its beam patterns to create a non-glare zone around vehicles, providing good long-range visibility for the driver without causing an uncomfortable glare for other road users. The performance of the ADB system is affected by the non-glare zone width. A narrow non-glare zone could create indirect glare in the side rearview mirrors of preceding vehicles during sharp turns while widening it results in poor road illumination. This research studies the trade-off relationship between glare and road illumination when altering the width of the non-glare zone in different driving scenarios. The study is conducted by using virtual driving simulation tools to simulate an ADB vehicle on four S-curve roads with minimum curvatures varying from 25 m to 100 m. Lux data are collected and processed using a fuzzy logic controller to mimic a human test driver to find the best non-glare zone width for balancing the trade-off. The research developed a design methodology allowing for a better understanding of the effect adjusting the width of the ADB non-glare zone has on ADB performance and improved ADB non-glare zone width optimum control system design.

Keywords: vehicle forward lighting; adaptive driving beam; non-glare zone; LucidDrive; fuzzy logic control; virtual night drive



Citation: Chen, Y.; Ahmadi, A.; Ahamed, M.J. Optimizing Non-Glare Zone Width of Adaptive Driving Beam (ADB) Using Fuzzy Logic Control. *Appl. Sci.* **2021**, *11*, 8840. <https://doi.org/10.3390/app11198840>

Academic Editor: Gabriella Tognola

Received: 18 August 2021

Accepted: 13 September 2021

Published: 23 September 2021

Publisher's Note: MDPI stays neutral with regard to jurisdictional claims in published maps and institutional affiliations.



Copyright: © 2021 by the authors. Licensee MDPI, Basel, Switzerland. This article is an open access article distributed under the terms and conditions of the Creative Commons Attribution (CC BY) license (<https://creativecommons.org/licenses/by/4.0/>).

1. Introduction

Automotive forward lighting is significant for driving safety, especially for night driving. An ideal forward-lighting system for vehicles should be able to provide adequate illumination of the road and surrounding area for the driver while not creating uncomfortable glares for other road users. Conventional vehicle forward-lighting systems have two fixed beam patterns: a high beam and a low beam. The high beam provides good long-range visibility to the driver, but it will create a strong glare for both oncoming and preceding vehicles. The low beam, however, minimizes the glare by sacrificing road illumination.

Adaptive driving beam (ADB) is an advanced vehicle forward-lighting system that automatically adapts its beam patterns to create a non-glare zone that includes both oncoming and preceding vehicles. Studies show that, in most driving scenarios, a vehicle equipped with ADB could provide the driver with road illumination equivalent to a high beam [1], while the glare it creates for other road users is similar to a vehicle with its low beam turned on [2,3]. Due to the limitations of the system, however, indirect glare in the rearview mirror was experienced in some sharp corners; an example of such a sharp corner is shown in Figure 1, in which the minimum curvature of the pointed S-curve is approximately 25 m. This limitation is caused by the nighttime vehicle recognition technology used in the ADB system. Due to poor lighting conditions at night, instead of recognizing the entire geometry of the vehicle, the camera in the ADB system recognizes vehicles only by the light projected from them [4,5]. Most of the nighttime vehicle detection

and recognition algorithms are based on the light's color [6–9] and symmetry [10,11], which differentiate the taillight of the vehicle from ambient lights. The boundary box is created based on such lamp recognition results to represent the vehicle. As a result, in the same direction sharp-cornering driving scenario, the rearview mirror will be moved away from the boundary box of the rear lamp during the maneuver. Indirect glare is created if the non-glare zone is not wide enough.

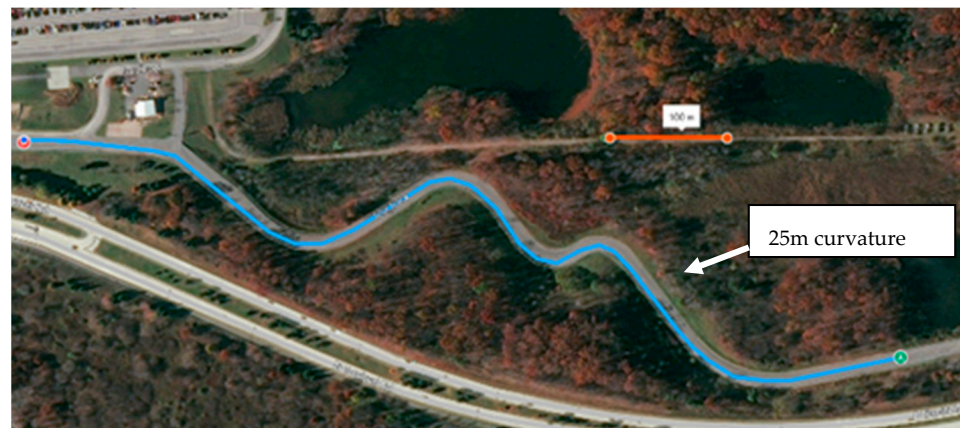


Figure 1. Example of a curvy road where indirect glare from the side rearview mirror is experienced by the preceding driver. ©2021 Microsoft Corporation, ©2021 TomTom.

This problem can be fundamentally solved if the geometry of the entire vehicle is recognized by the system instead of just its light. The deformable part model (DPM) has been used for object recognition in good lighting conditions. Tehrani et al. [12] improved the performance for vehicle detection at night using DPM with a lateral filter that allows the system to recognize the vehicle geometry in low-lighting conditions. Zeng et al. [13] presented a vehicle recognition algorithm with low-light enhancement with artificial intelligence and machine learning. Balci et al. [14] proposed an approach for images captured at nighttime that uses near-infrared camera images with deep learning. Those algorithms show the potential of such detection being used for future ADB systems. Another solution is to predict the maneuver of the stimulus vehicle using sensor fusion. Götz et al. [15] improved the ADB system using sensor fusion and predictive algorithms in twisting roads and passing-car scenarios. In the field of adaptive forward-lighting systems (AFS), Gao and Li [16] studied eye-tracking technology, and Bradai [17] presented a navigation-based virtual sensor for the AFS. Those predictive technologies could also be applied in mitigating the glare issue for ADB. Choi et al. [18] designed laser diode scanning to improve the resolution of ADB; combined with those additional inputs, the non-glare zone can be projected more precisely to avoid glare while maximizing illumination.

Each such improvements of ADB require additional hardware for the system or a more advanced algorithm. With the currently existing system, this problem can also be solved by widening the non-glare zone, though at the cost of road illumination. The question is how to find the best non-glare zone width to balance the issue of glare and road illumination. This research aims to provide automakers with a guideline for the fine-tuning of the current ADB system by adjusting the non-glare zone width. The research is conducted on a virtual night drive simulator called LucidDrive and presents a proof of concept for using fuzzy logic control to mimic a human test driver in finding the best non-glare zone width.

2. Modeling: Night Drive Simulator

This research is conducted on LucidDrive, a night drive simulator. Compared to physical tests and experiments, not only is the cost of a virtual night drive much lower, but it is also not limited by testing vehicles, types of roads, or weather conditions. Additionally, due to the current legislation status of ADB in America, access to ADB vehicles is limited. As a result, a virtual night drive simulator was preferable in performing this study.

The first step of the research is to reproduce the ADB system and the side rearview mirror glare problem in the night drive simulator. The simulator provided two approaches for simulating the ADB function within the Adaptive Forward-Lighting System (AFS) plug-in of the software: pixel masking and matrix beam [19]. The pixel-masking algorithm simulates an ideal high-definition ADB system allowing for precise control of the non-glare zone’s shape. The pixel-masking algorithm creates a virtual mask in front of the lamp to shade out the non-glare zone according to the shape of the boundary box. In the other approach, the matrix beam algorithm simulates a more realistic ADB system, with each segment having an individual beam pattern file. If the boundary box is within a certain region, the corresponding segment will be turned off. The shape of the non-glare zone is limited by the numbers and the beam patterns of the LEDs. As the resolution of the matrix headlamp increases, the difference in performance between these two approaches will reduce, yet pixel masking is computationally cheaper, as it only needs one beam pattern file. The comparison is shown in Figure 2.

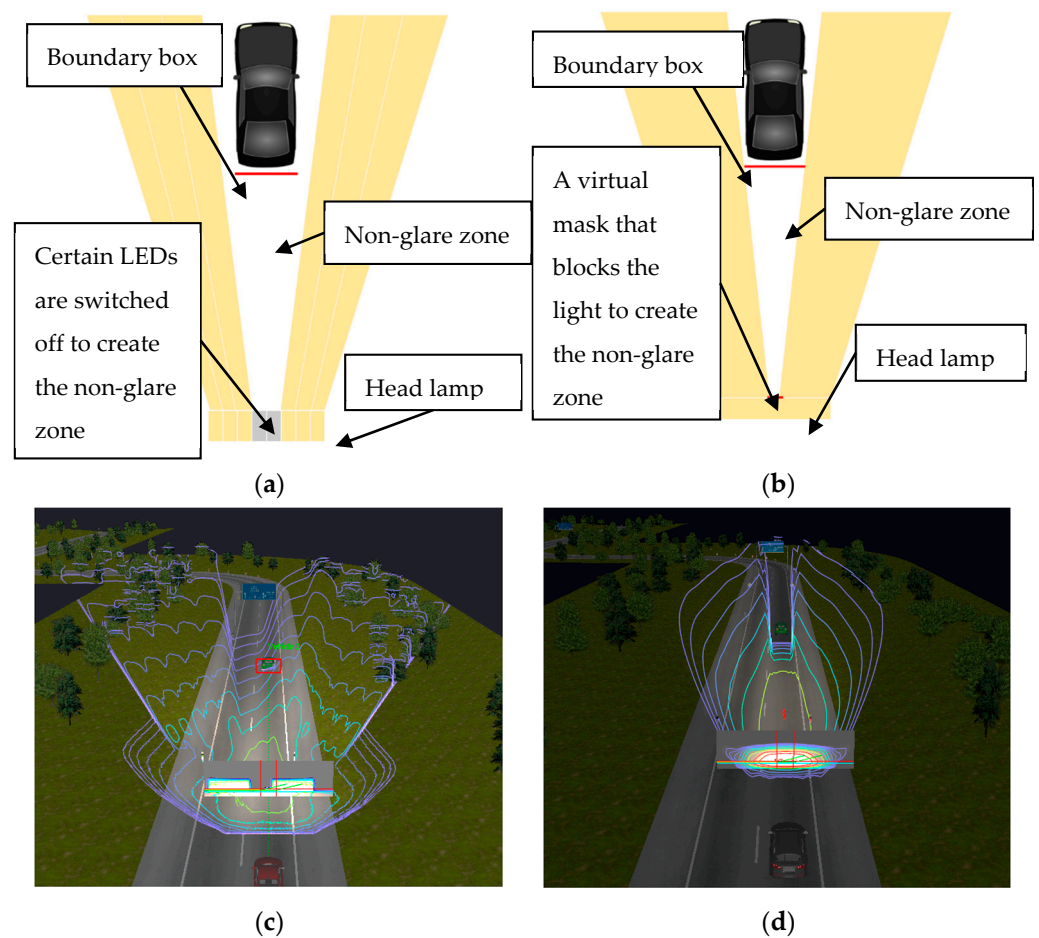


Figure 2. Comparison of pixel masking and matrix beam showing the difference of two simulation algorithms: (a,c) ADB simulation using matrix beam algorithm, in which each segment can be switched on/off individually; (b,d) ADB simulation using pixel-masking algorithm, which uses one beam pattern, with the boundary box of the stimulus vehicle masked out.

For more accurate control of the width of the boundary box and a better illustration of the trade-off relationship between the indirect side rearview mirror and road illumination, the pixel-masking script is chosen to simulate ADB in this research. The beam pattern that is being used in this research is a combined eight-element segmental LED lamp.

2.1. Night Driving Model Development

The built-in AFS simulation module recognizes the stimulus vehicle as a three-dimensional boundary box. In this case, glare will never be created, which is ideal but not realistic. Since, in reality, only the taillight of the stimulus vehicle is recognized by the system, the boundary should be two-dimensional and surround the rear face of the vehicle, so a modification of the script is needed. Figure 3 provides a graphical comparison between the original and the modified ADB simulation, in which the ADB beam pattern, stimulus vehicle, and road geometry along all driving parameters are identical. The non-glare zone width in both simulations is set at 100% of the boundary box. Images (a) and (c) are the original three-dimensional boundary box, and images (b) and (d) show the resultant boundary box after modification, which is a two-dimensional plane parallel to the rear of the vehicle that can better simulate real driving scenarios. From the comparison of the driver views, it can be observed that, with the modification, the side rearview mirror (circled in green) that was originally included in the non-glare zone (Figure 3a) is now exposed in the glare zone (Figure 3b), highlighted with the red circle. It can also be observed from the top view, although the non-glare zone setting is the same as 100%; with the modification of the boundary box, the resultant non-glare zone is significantly narrower. As a result, the frontal part of the stimulus vehicle is exposed (Figure 3d), compared with Figure 3c, in which the entire vehicle is in the non-glare zone. This indicates the glare issue is successfully reproduced in the simulation with the modification.

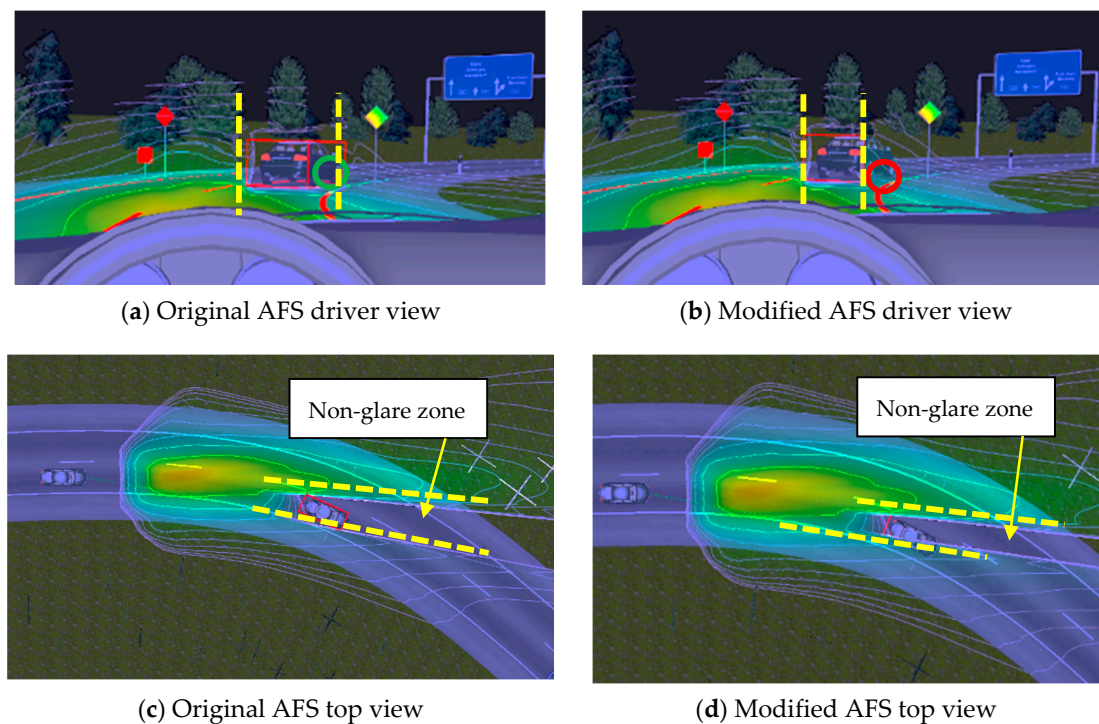


Figure 3. A graphical comparison in the simulator between the original and the modified ADB simulation, in which the non-glare zone is set at 100% and all parameters are identical. The red lines around the stimulus vehicle represent the boundary box: (a,c) The original ADB simulation in which the three-dimensional boundary box is recognized, and, thus, the entire vehicle geometry is covered by the non-glare zone. The modification in (b,d) simulates a more realistic ADB, in which only the taillight is recognized; thus, in top view (d), it is just a line at the rear of the stimulus vehicle. The non-glare zone is highlighted with yellow dashed lines showing that, with the modification, the side rearview mirror will be excluded from the boundary box during the cornering maneuver. The comparison shows that the simulator's modified AFS plug-in can reproduce the glare issue.

Figures 4 and 5 demonstrate how altering the non-glare zone width would affect glare and road illumination by comparing an ADB with a 100% non-glare zone to one with 150% in the same driving scenario. The width of the non-glare zone is measured as the

percentage with respect to the width of the boundary box. A 100% non-glare zone width means it is the same width as the boundary box, which is the narrowest; a 150% non-glare zone width means it widens (equally on both the left and right) to 150% of the boundary box width. In Figure 4a, the rearview mirror, highlighted in the red circle, is not covered by the non-glare zone, and, thus, glare is created. By increasing the non-glare zone width to 150% of the boundary box, shown in Figure 4b, glare is eliminated in the rearview mirror, highlighted in a green circle, indicating a good experience. Meanwhile, in terms of road illumination, with a 100% non-glare zone width, the two circled street signs in Figure 5a are illuminated, while Figure 5b shows that they are not in a widened non-glare zone, indicating worse road illumination. This shows that, although widening the non-glare zone could solve the side rearview mirror’s indirect glare issues, the narrower non-glare zone provides better visibility to the driver, who can observe the surrounding environment and road conditions more effectively. For example, if a deer is standing by the roadside, the ADB system with a narrower non-glare zone will illuminate the deer sooner, giving the driver more reaction time, thus enhancing driving safety. This comparison indicates the importance of defining the best non-glare zone width that balances glare mitigation and driver visibility.

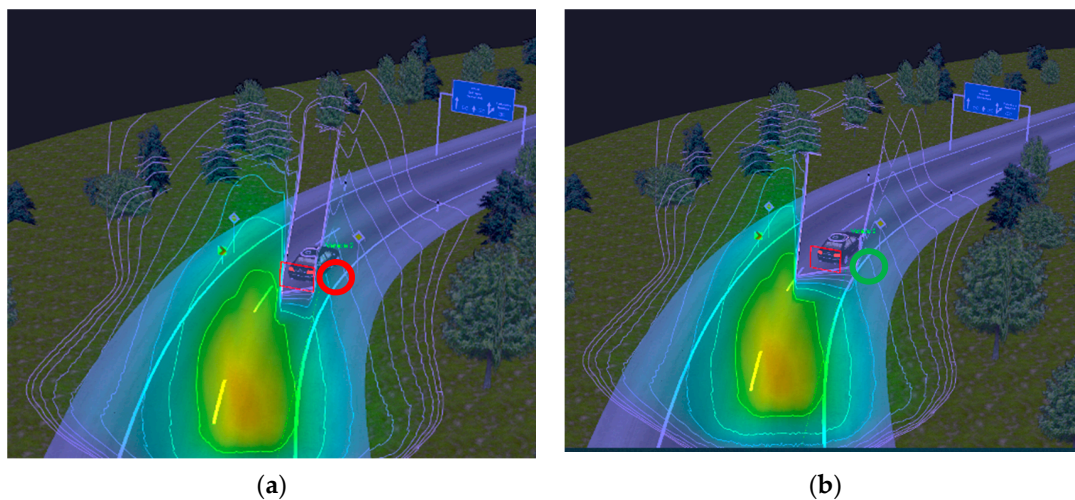


Figure 4. Effect on glare when altering non-glare zone width, showing that widening the non-glare zone could effectively eliminate glare: (a) 100% non-glare zone width (glare); (b) 150% non-glare zone width (no glare).

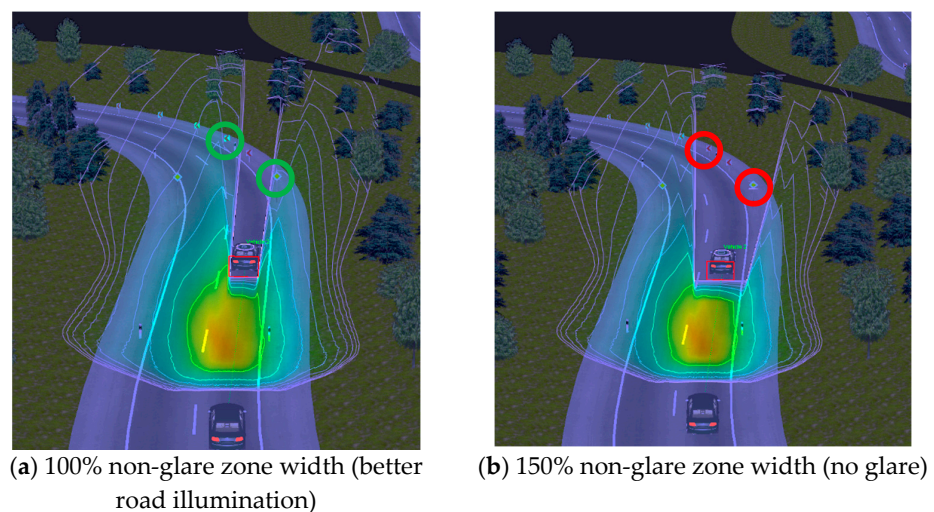


Figure 5. Effect on road illumination when altering the non-glare zone width, showing that a widened non-glare zone sacrifices road illumination. For example, the traffic signs circled on (a) are well illuminated;

however, when the non-glare zone increases on (b), the signs are included in the non-glare zone and, thus, are not illuminated. This indicates the driver will have better and wider visibility with the narrower non-glare zone, which enhances driving safety.

2.2. Driving Scenario Design

Four S-curve driving scenarios are designed, which are shown in Figure 6. The designs are based on the road shown in Figure 1. All four S-curves are designed with a track transition curve [20] with a minimum curvature of 25 m, 50 m, 75 m, and 100 m. Those curvature designs are based on the speed of the ADB vehicle, calculated by the formula (1) of the curve design guideline provided by the AASHTO Green Book [21].

$$R_{min} = \frac{V_d^2}{127(e + f_{max})} \quad (1)$$

where:

- R_{min} is the minimum curvature;
- V_d is the advisory speed;
- e is the superelevation, which is 0 in this case, as suggested by NHTSA for ADB testing in NPRM [22]; and
- f_{max} is the comfortable side friction factor referenced from the Green Book [23].

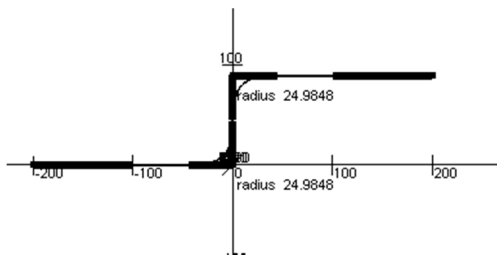
The 100 m curvature corresponds to a genetic ADB activation speed of 45 km/h, which is also the minimum curvature that NHTSA proposed for ADB testing. The ADB function of the most current production vehicle will automatically be activated when the vehicle speed exceeds the activation speed. The deactivation speed of ADB, however, is usually lower than the activation speed. A study from NHTSA shows that ADB deactivation speed can be as low as 25 km/h [24]. Thus, if a vehicle traveling with ADB enabled encounters a curve with a curvature as low as 25 m, the ADB will not be deactivated. The 50 m and 75 m curves are included to study the influence of curvature on optimized non-glare zone width.

The following distance between the two vehicles is calculated by the three-second rule, suggested by the National Safety Council of the United States [25], assuming there are safe driving conditions. The complete set of parameters of the four driving scenarios for this research are shown in Table 1.

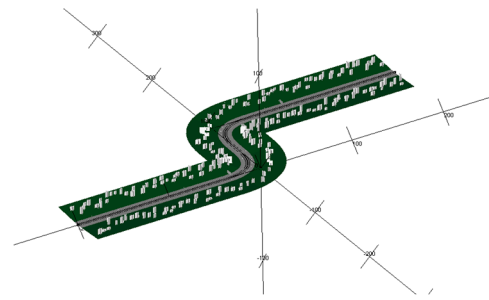
2.3. Virtual Stimulus Vehicle and Light Sensor

Out of the box, LucidDrive is not designed for and not capable of performing data collection. A new virtual light sensor was implemented in the software for this research. The method involves calculating the relative position of the sensor point to the ADB head beam then extracting data from the beam pattern file. Compared to real-time ray tracing, this method is less time-consuming and computationally cheaper while still accurate.

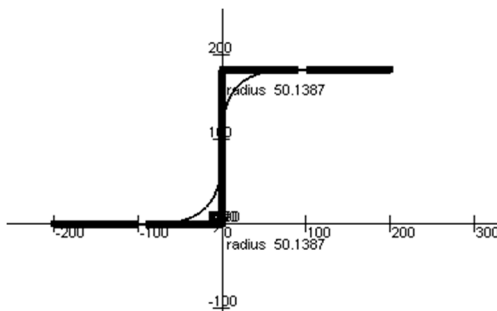
The selection of a stimulus vehicle and sensor position in this research is based on the SAE J3069 [26] ADB test fixture. A Mercedes E W211 vehicle geometry is chosen as the stimulus vehicle, considering that its dimensions are similar to the test fixture. The light sensor is mounted 0.9 m above the ground, 0.9 m away from the center along the y -axis, and 3.5 m away from the rear of the vehicle along the x -axis, representing the position of the driver-side rearview mirror, illustrated in Figure 7.



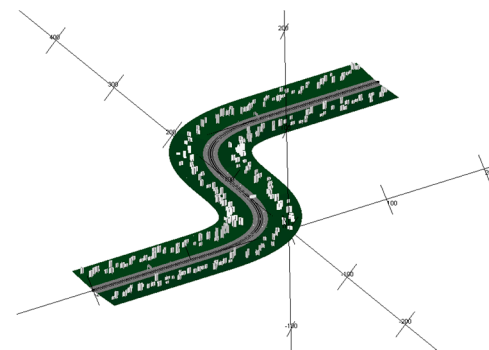
(a) Planar graph of S-curve with minimum curvature at 25 m



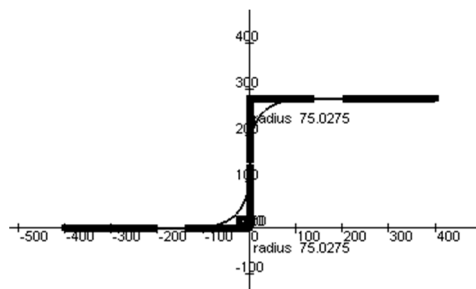
(b) Rendering of S-curve with minimum curvature at 25 m



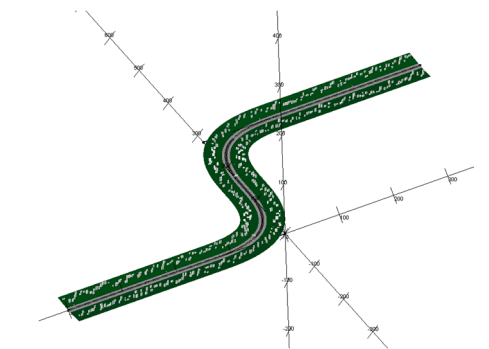
(c) Planar graph of S-curve with minimum curvature at 50 m



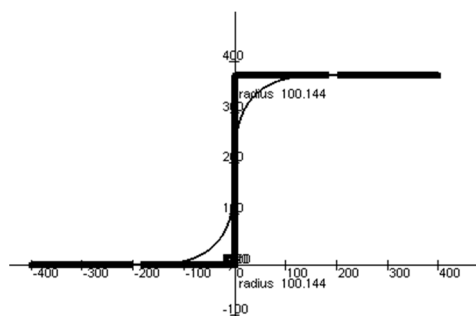
(d) Rendering of S-curve with minimum curvature at 50 m



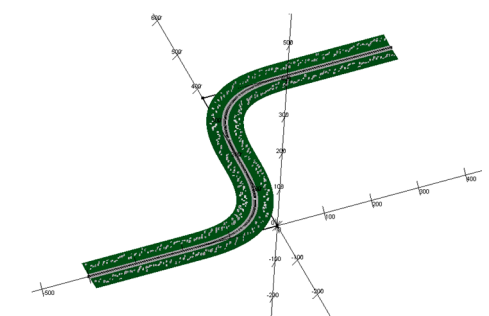
(e) Planar graph of S-curve with minimum curvature at 75 m



(f) Rendering of S-curve with minimum curvature at 75 m



(g) Planar graph of S-curve with minimum curvature at 100 m



(h) Rendering of S-curve with minimum curvature at 100 m

Figure 6. Driving scenarios prepared for the virtual night drive data collection. The curve varies from 25 m to 100 m, with the 25 m curvature corresponding to a vehicle traveling at minimum ADB deactivation speed, below which the ADB will automatically be deactivated and switch to low beam. The 100 m curvature corresponds to the minimum curvature that NHTSA proposed for ADB testing in NPRM [22].

Table 1. Parameters of the driving scenario.

Curvature [m]	Side Friction Coefficient [-]	Speed [km/h]	Rounded Speed [km/h]	Following Distance [m]
25	0.18	23.9	25	20
50	0.17	32.8	30	25
75	0.17	40.2	40	30
100	0.16	45.1	45	40

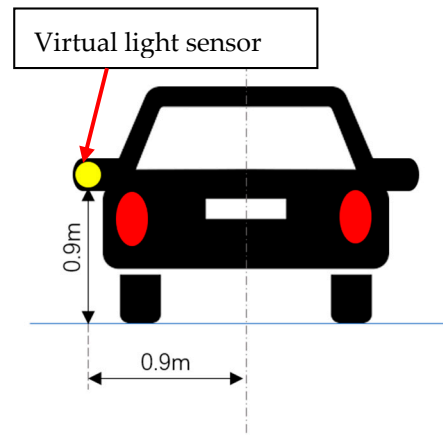


Figure 7. The position of the virtual light sensor, which corresponds to the ADB test fixture from SAE J3069 [26].

3. Data Collection and Post-Processing

3.1. Data Acquired from LucidDrive

In each driving scenario, the vehicle starts from the left end of the road, then navigates a left turn followed by a right turn and finishes at a straight road. Because the overall length of the road also increases when the curvature increases, the simulation time varies from around one to two minutes. The lux reading of each simulation is logged, and a lux–time graph is plotted. Figure 8 shows the data collected for the narrowest non-glare zone in the first driving scenario in which the minimum curvature is 25 m.

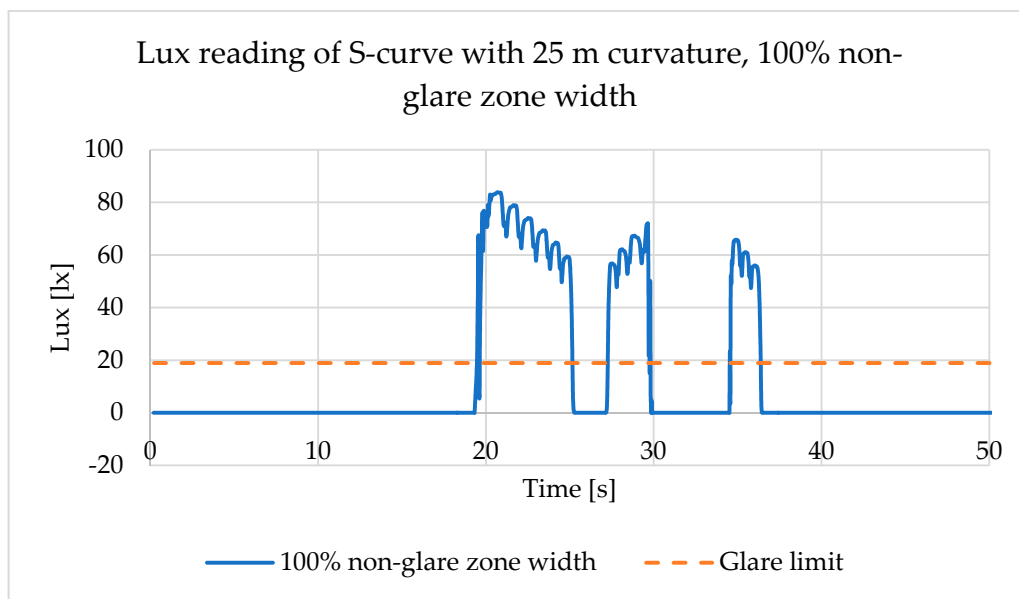


Figure 8. Lux reading of S-curve with 25 m curvature simulation at 100% non-glare zone width. The dashed line is 18.9 lux, above which is considered to be glare, according to both NHTSA [22] and SAE [26].

At the beginning of the simulation, between 0 and 20 s, the vehicle travels on a straight road (Figure 9a), where zero glare is created. When the stimulus vehicle enters the corner at around 20 s (Figure 9b), the side rearview mirror shifts away from the non-glare zone, and, thus, glare is created, which is reflected as the first spike on the lux–time graph. As the vehicle continues the left turn (Figure 9c), there is a brief time when the stimulus vehicle exits the high beam zone of the test vehicle during which the lux reading drops to zero for a few seconds; then, glare is again observed when the test vehicle enters the corner, reflected in the graph as the second spike. When the vehicle enters the right turn, no glare should be created from the driver-side rearview mirror since the light is blocked by the vehicle body (Figure 9d). The third spike in the lux–time graph is due to the limitation of the simulator—its lack of ray-tracing technology—causing the light to reach the sensor by penetrating through the vehicle geometry. This is considered an error and will be neglected during data processing.

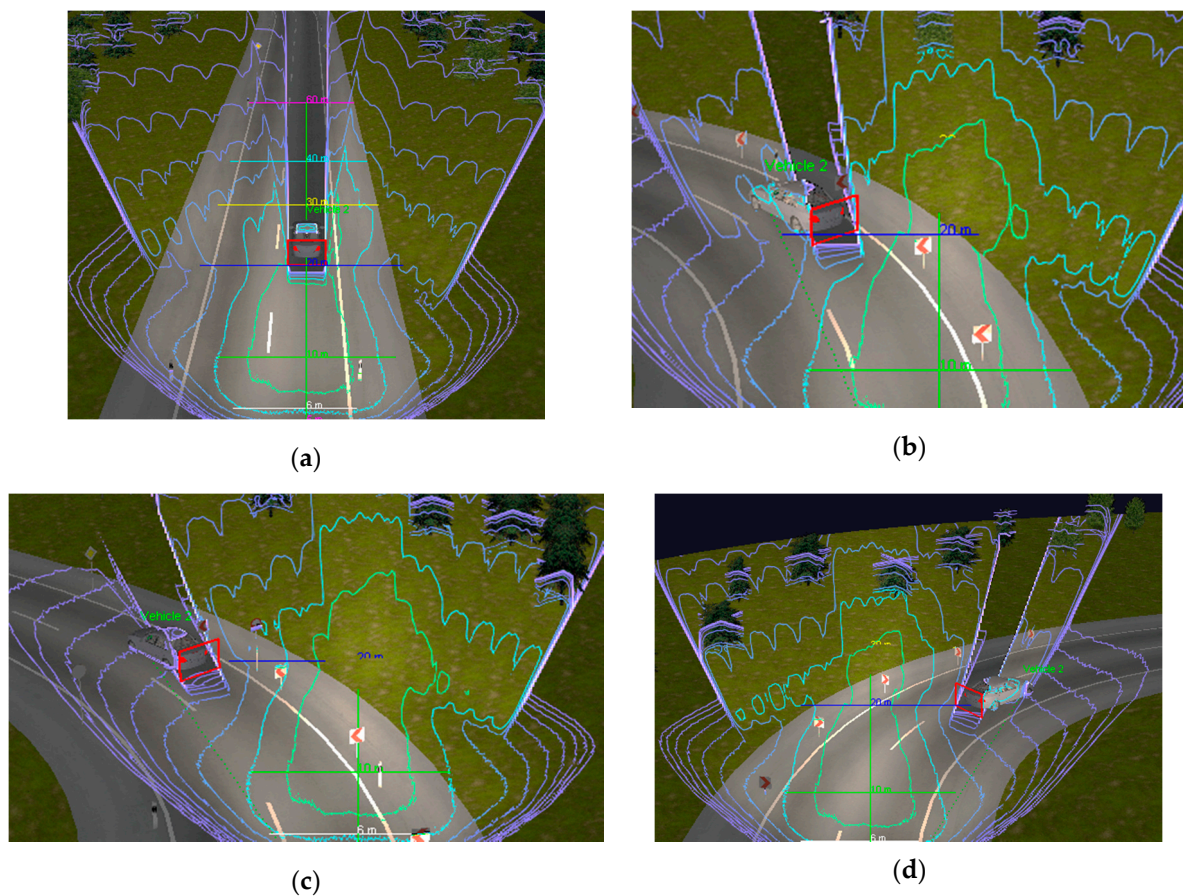


Figure 9. S-curve with 25 m curvature simulation at 100% non-glare zone width: (a) At the beginning of the simulation, the vehicle travels on a straight road, and no glare is created. (b) When the vehicle enters the corner, glare is created, corresponding to the first peak in Figure 8. (c) When the stimulus vehicle exits the high beam area, there is a short time when glare drops to zero, corresponding to the area between two peaks in Figure 8. (d) Light penetrates through the vehicle body due to the limitation of the simulator, which is shown as the third peak in Figure 8 and is neglected as an error.

In accordance with the NHTSA ADB testing proposal [22] and the SAE standard ADB testing procedure [26] and for the same direction driving scenario at a distance shorter than 60 m, lux readings above 18.9 lx are considered to be glare, which is the dashed line in Figure 8. In this project, the total time during a simulation when the lux reading is above 18.9 lx is considered as the glare rating for this driving scenario and will be used as an input in the fuzzy logic controller to find the best non-glare zone width.

As shown in Figure 10, with increases in non-glare zone width, not only does the total glare time reduce (shown in Figure 11), but also the lux peak reduces. It is noted that when the non-glare zone increases from 140% to 180%, the second lux peak (around 27 s to 30 s) is eliminated. Finally, when the non-glare zone width is increased to 265% of the boundary box width, all lux readings are below the 18.9 lx limit, so glare can be considered to be eliminated. The upper limit of the non-glare zone width for a 25 m curvature cornering driving scenario when road illumination is the worst is considered to be 265%.

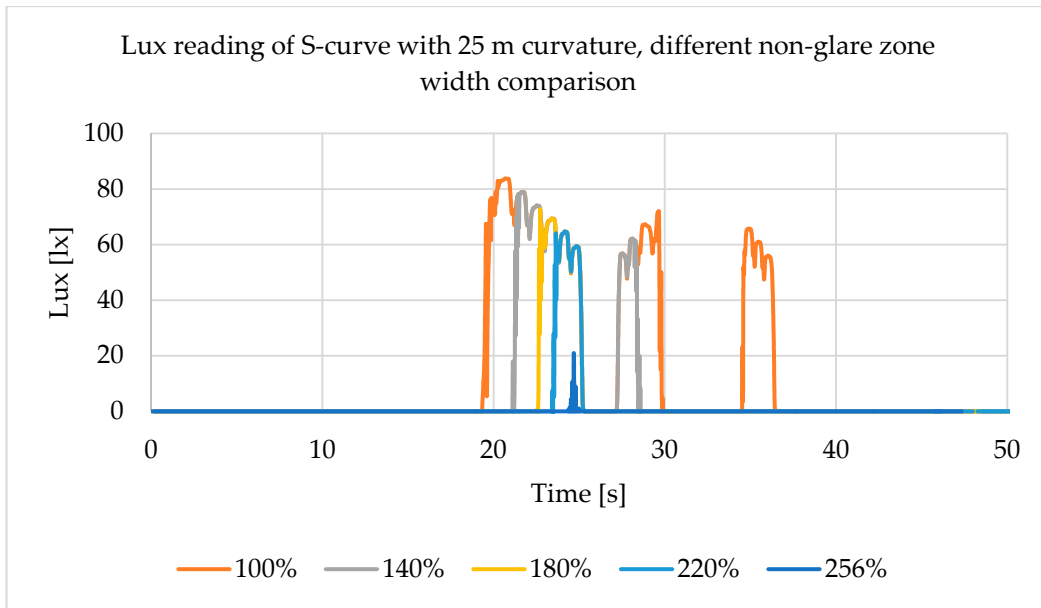


Figure 10. Lux reading of S-curve with 25 m curvature simulation in different non-glare zone widths, showing the trend of reduction in glare with increasing non-glare zone width.

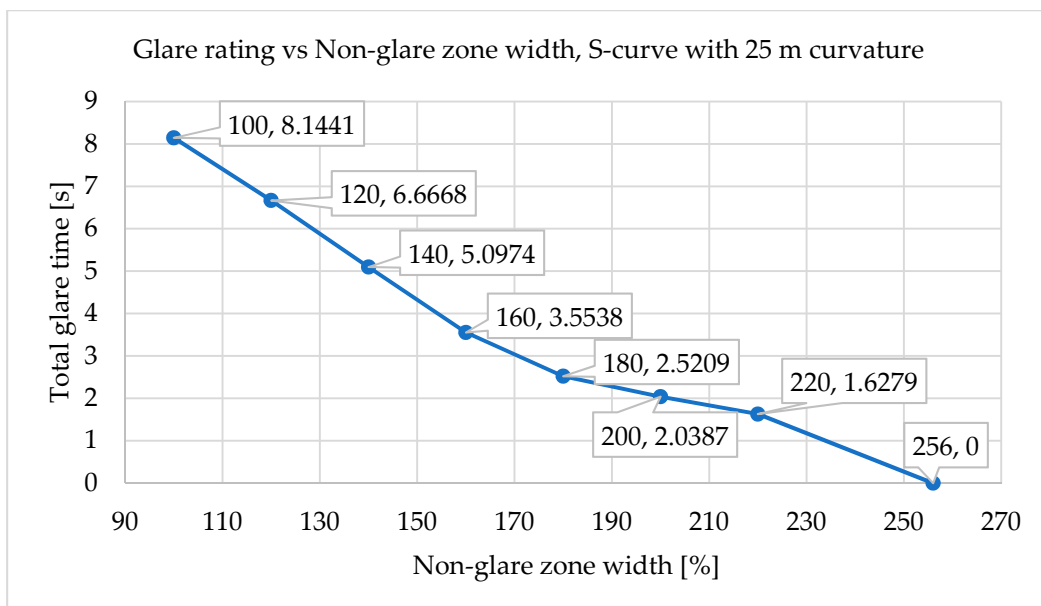


Figure 11. Total glare time vs. non-glare zone width for S-curve with 25 m curvature, showing that the total glare time reduces with increasing non-glare zone width. All glare is eliminated if the non-glare zone widens to 265% of the boundary box width.

3.2. Fuzzy Logic Controller

Fuzzy logic was first introduced in 1965 by Zadeh [27]. It is designed to handle the concept of partial truth, which is close to human semantic statements in which the truth is mostly partial and imprecise. Unlike classical logic that operates at either true or false, fuzzy logic operates with continuous values between the two extremes: completely true and completely false. Similar to how the color gray is found between black and white, fuzzy logic can present imprecise linguistic expressions such as “slightly”, “quite”, or “very”. Fuzzy logic has been employed in many applications such as temperature control of air conditioners and suction power control in vacuum cleaners, amongst others.

The data acquired from the simulator is then processed in MATLAB with a Fuzzy Logic Toolbox [28]. This project aims to provide automotive OEMs with an efficient and less time-consuming methodology for studying ADB non-glare zone width. Considering the use of a human test driver to evaluate the performance of a vehicle headlamp, both glare and road illumination cannot be precisely stated between just two opinions: good or bad. Choosing the best value of the non-glare zone width that balances the glare and road illumination is not a dichotomous situation. A fuzzy logic controller is a good candidate to mimic a human test driver in providing feedback and finding the best value in this application, as it not only takes continuous input but also does not require a precise mathematical model or a large volume of data. Instead, it is simply based on logic, making it less time-consuming and less computationally expensive.

As shown in Figure 12, the two inputs to the controller are the glare rating and the road illumination rating. The glare rating is represented by the overall time that the lux reading is above the glare limit in a simulation, as discussed in the previous section. The road illumination rating can be represented by the non-glare zone width; this is because the road illumination is at its best when the non-glare zone is at its narrowest and at its worst when the non-glare zone is at its widest. Thus, they can be seen as inversely proportional. The wider the non-glare zone, the less area that is covered by the high beam area that benefits from the dynamic beam pattern of the ADB. The output of the controller is the change in non-glare zone width.

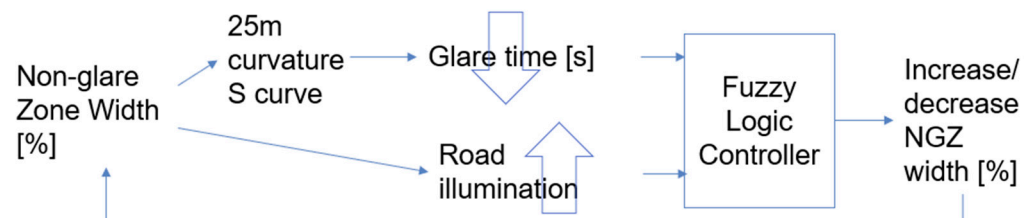


Figure 12. Schematic showing fuzzy logic controller block diagram.

Both inputs use two membership functions to represent good and bad performance. The “good” membership functions represent a low glare time and a narrow non-glare zone that results in good road illumination, while the “bad” membership functions represent the opposite. The output uses three membership functions to indicate that the non-glare zone width should be increased, decreased, or if it is just good. The fuzzy logic controller is based on three rules:

- If both road illumination and glare are good, then the non-glare zone width is good.
- If the road illumination is poor while the glare is good, the non-glare zone width should be increased.
- If the road illumination is good, while the glare is poor, then the non-glare zone width can be reduced.

Two trials are presented in this research using different basic membership functions to find the best non-glare zone width. The first trial uses linear triangular membership functions, and the second trial uses Gaussian membership functions, as shown in Figure 13. The parameters of the unscaled membership functions are shown in Table 2. The range

of the inputs is considered as spanning from the worst case to the best case. For input on the road illumination, the best case is when the non-glare zone is at its minimum, which is 100% of the width of the boundary box; the worst case is when it is the widest, with all glare eliminated in all driving scenarios, which is 256% of the boundary box width. For the glare rating, the worst case is the overall glare duration at the 100% non-glare zone width at each driving scenario, while the best case is 0 s of glare, indicating that it is glare-free. These details are shown in Table 3. This research aims to demonstrate the methodology of using fuzzy logic to mimic human feedback. The parameters can be seen as an initial gauss and would require a physical test for fine-tuning, which is considered to be future work and not included in this research. The parameters are also expected to vary from case to case with different ADB systems and different beam patterns.

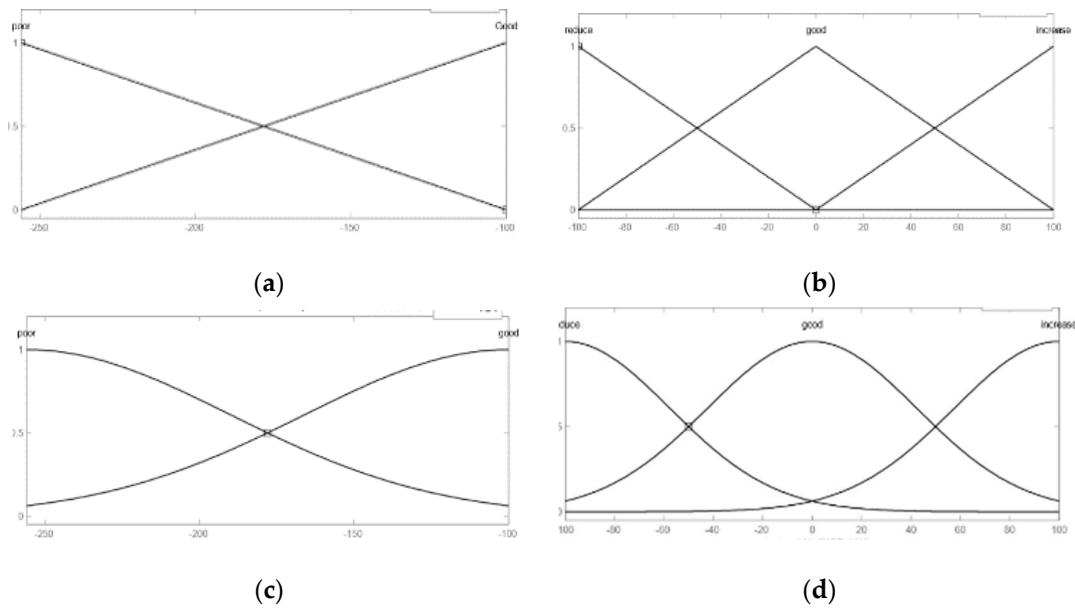


Figure 13. Membership function of fuzzy logic controller: (a) road illumination input triangular membership function in Trial 1; (b) change in non-glare zone width output triangular membership function in Trial 1; (c) road illumination input Gaussian membership function in Trial 2; (d) change in non-glare zone width output Gaussian membership function in Trial 1.

Table 2. Parameters of the unscaled membership functions, range 0–1.

Function names	Input			Output	
	good	bad	increase	good	decrease
Trimf parameters	[0, 1, 2]	[−1, 0, 1]	[0.5, 1, 1.5]	[0, 0.5, 1]	[−0.5, 0, 0.5]
Gaussmf parameters	[0.4247, 1]	[0.4247, 0]	[0.2123, 1]	[0.2123, 0.5]	[0.2123, 0]

Table 3. Variable range of the membership functions.

Driving Scenario	Input		Output
	Glare	Road Illumination	Change in Non-Glare Zone Width
S-curve with 25 m curvature	0–8.144	100–256	−100–100
S-curve with 50 m curvature	0–14.686		
S-curve with 75 m curvature	0–15.047		
S-curve with 100 m curvature	0–9.61		

The iteration of the optimization in four driving scenarios is shown in Tables 4 and 5, in which the last column are the outputs from the fuzzy logic controller, which were added to the non-glare zone width for the next iterations. The best non-glare zone width is taken when the output change in non-glare zone width is less than 0.5%. The two demonstrated trials show different iteration. Trial 1 took four to five iterations to converge to the optimal glare-free zone, while Trial 2 took six to seven iterations. This shows that different types of membership functions are able to converge to an optimal non-glare zone. A correlation study of physical tests would help to select the membership function type and its parameter in future work.

Table 4. Trial 1 iteration of four driving scenarios, using the fuzzy logic controller with linear membership function.

Driving Scenario	Iteration	Non-Glare Zone Width [%]	Glare Rating [s]	Output [%]
S-curve with 25 m curvature	1	256	0	−105
	2	151	4.2	−2.3
	3	149	4.4	−0.53
	4	148	4.5	−0.06
S-curve with 50 m curvature	1	180	0	−20
	2	160	3	−7.93
	3	152.3	4.6	−0.885
	4	151	4.8	−0.008
S-curve with 75 m curvature	1	154	0	−9.34
	2	144.7	1.7	−5.2
	3	138.4	3.1	−1.17
	4	137.2	3.6	−0.23
	5	137	3.6	0.274
S-curve with 100 m curvature	1	143	0	−3.87
	2	139.1	1.1	−2.82
	3	136.3	1.2	−2
	4	134.3	1.8	−0.785
	5	133.5	1.9	−0.5

Table 5. Trial 2 iteration of four driving scenarios, using the fuzzy logic controller with Gauss membership function.

Driving Scenario	Iteration	Non-Glare Zone Width [%]	Glare Rating [s]	Output [%]
S-curve with 25 m curvature	1	256	0	−55.7
	2	200.3	2	−25.1
	3	175.2	2.6	−7.09
	4	168.11	3.1	−2.36
	5	165.75	3.2	−1.86
	6	163.89	3.4	0.367
S-curve with 50 m curvature	1	180	0	−13.9
	2	166.1	2	−7.6
	3	158.5	2.6	−4.86
	4	153.64	4.2	−1.64
	5	152	4.3	−1.13
	6	150.87	4.5	−0.308
S-curve with 75 m curvature	1	154	0	−4.74
	2	149.26	1	−3.54
	3	145.72	1.6	−2.75
	4	142.97	2.2	−2
	5	140.97	2.6	−1.44
	6	139.53	2.8	−1.15
	7	138.38	3.1	−0.67
S-curve with 100 m curvature	1	143	0	−2.62
	2	140.38	0.5	−2.16
	3	138.22	0.9	−1.71
	4	136.51	1.22	−1.3
	5	135.21	1.4	−1
	6	134.21	1.6	−0.7
	7	133.51	1.75	−0.45

4. Result and Discussion

Table 6 and Figure 14 show the result of the best non-glare zone width in different driving scenarios. The x-axis is the minimum curvature of the driving scenario, and the y-axis is the best non-glare zone width defined by the fuzzy logic controller. The top dashed line is the non-glare zone width when all glare is eliminated, which is in the extreme case of the best glare rating and the worst road illumination. The x-axis also represents the narrowest non-glare zone width, which is just as wide as the vehicle boundary box, when the road illumination rating is the best and the glare rating is the worst. The best value of the non-glare zone width should lie between these two lines, balancing the glare/road illumination trade-off. The two solid lines are the first and second trials of the fuzzy logic controllers using different membership functions. Those can be considered two balances of the road illumination and glare trade-off. Those two trials have very similar results, except in the S-curve with 25 m minimum curvature, in which the second trial prefers lower glare and the first one prefers better road illumination.

Table 6. Best non-glare zone width vs. minimum curvature of the S-curve in all four driving scenario simulations.

Driving Scenario	Minimum Curvature [m]	Trial 1 Optimal Non-Glare Zone Width [%]	Trial 2 Optimal Non-Glare Zone Width [%]	Glare-Free Non-Glare Zone Width [%]
1	25	148	164	256
2	50	151	150	180
3	75	137	138	154
4	100	133	133	143

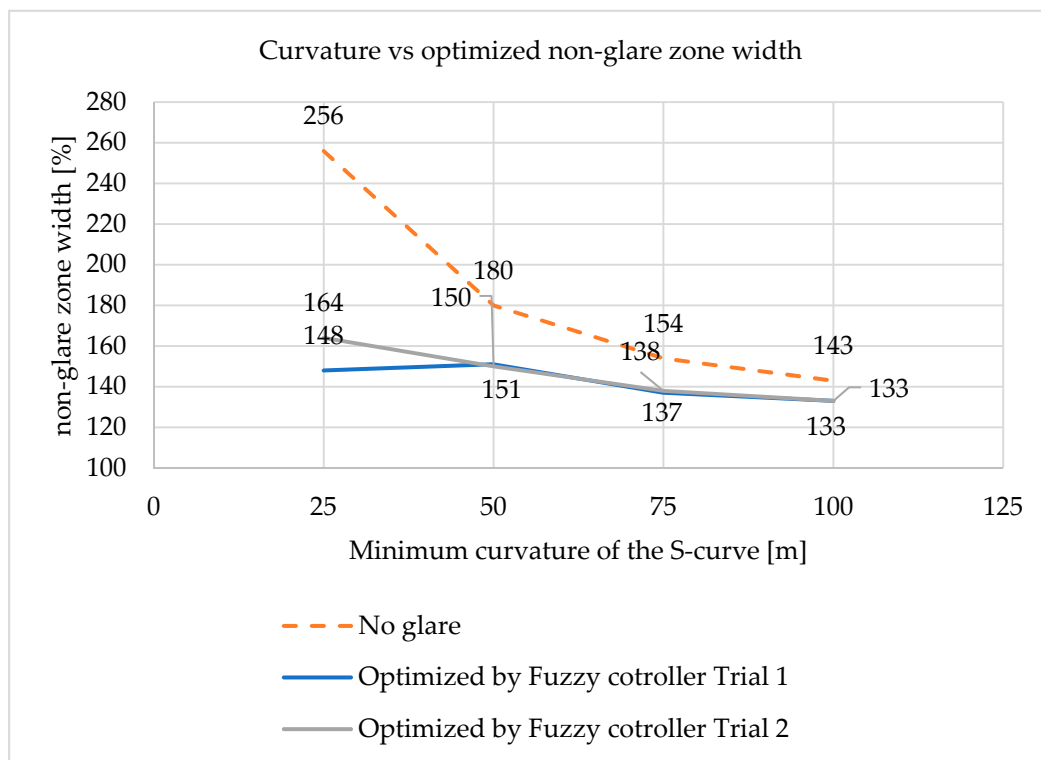


Figure 14. The minimum curvature in the driving scenario vs. best non-glare zone width.

Such results could be used as an ADB non-glare zone width design guideline for automotive OEMs. For example, if an OEM would like to consider the performance of this ADB system at corner curvature as low as 50 m, the non-glare zone width should be set at 151% of the boundary box according to the result, balancing the glare and road illumination. Note that the minimum curvature proposed by NHTSA for ADB testing in NPRM is 100 m. If the proposed ADB testing procedure is executed, then the minimum non-glare zone width of this ADB should be set to 143% of the boundary box to meet the legal requirement.

5. Conclusions

Adaptive driving beams enhance night driving safety by providing high-beam-level road illumination while eliminating the uncomfortable glare that a normal high beam would create for other road users. Due to the limitation of the current vehicle recognition method, indirect glare through side rearview mirrors was observed by the vehicle tailed by an ADB vehicle at sharp corners.

This research focuses on a solution to this issue by providing automotive OEMs with a methodology to develop a design guideline for non-glare zone width adjustment. This research demonstrates a novel methodology to study the trade-off effect between road

illumination and glare when tuning the non-glare width in different driving scenarios using a virtual night drive simulator and fuzzy logic control to find the non-glare zone width. Experimenting with a virtual simulator avoids the difficulty and limitations of conventional night drives. The simulation result shows the minimum ADB non-glare zone width to eliminate all glare at S-curves with minimum curvatures at 25 m, 50 m, 75 m, and 100 m. The fuzzy logic controller mimics a human test drive to provide feedbacks and balances with the loss of road illumination and the reduction in glare time, converging them to an optimal width. The research also demonstrates fuzzy logic controllers with two basic membership functions, and both of them converge to a similar optimal non-glare zone width in each driving scenario. The demonstration uses a genetic beam pattern to prove the concept. By replacing the generic beam pattern file with a specific ADB beam pattern, a physical test could be conducted to validate the result from the night drive simulator. The physical test should also collect glare and road illumination feedbacks from the driver, which will be used to select the membership function types and tune the parameters of the fuzzy logic controller.

Author Contributions: All authors contributed equally. All authors have read and agreed to the published version of the manuscript.

Funding: This research was funded by MITACS, grant number IT18512.

Institutional Review Board Statement: Not applicable.

Informed Consent Statement: Not applicable.

Data Availability Statement: Data is contained within the article.

Acknowledgments: The authors would like to thank MITACS for funding support and Stellantis N.V. Canada for their financial support. We thank Guido Albertengo from Politecnico di Torino; Dennis Novack and Davide Secchiero from Stellantis for their discussions, guidance, and support for this project. We also thank the support from Sida Li and Steven Simic, as well as the Automotive Research and Develop Center (ARDC) in Windsor, Ontario.

Conflicts of Interest: The authors declare no conflict of interest.

References

1. American Automobile Association. *Comparison of European and U.S. Specification Automotive Headlamp Performance*; American Automobile Association: Heathrow, FL, USA, 2019.
2. Neumann, R. Adaptive Driving Beam-Visibility Improvement versus Glare. In *SAE Technical Paper*; SAE International: Warrendale, PA, USA, 2014. [CrossRef]
3. Reagan, I.; Brumbelow, M. Perceived Discomfort Glare from an Adaptive Driving Beam Headlight System Compared with Three Low Beam Lighting Configurations. *Procedia Manuf.* **2015**, *3*, 3214–3221. [CrossRef]
4. Luo, F.; Hu, F. A comprehensive survey of vision based vehicle intelligent front light system. *Int. J. Smart Sens. Intell. Syst.* **2014**, *7*, 701–723. [CrossRef]
5. Valeo MatrixBeam-046834-046835-Technical Bulletin. Available online: <https://www.valeoservice.com/en-com/techassist/technical-bulletin/valeo-matrixbeam-046834-046835> (accessed on 6 July 2021).
6. López, A.; Hilgenstock, J.; Busse, A.; Baldrich, R.; Lumbreras, F.; Serrat, J. Nighttime vehicle detection for intelligent headlight control. In *Advanced Concepts for Intelligent Vision Systems*; Springer: Berlin/Heidelberg, Germany, 2008; pp. 113–124.
7. O'Malley, R.; Jones, E.; Glavin, M. Rear-lamp vehicle detection and tracking in low-exposure color video for night conditions. *IEEE Trans. Intell. Transp. Syst.* **2010**, *11*, 453–462. [CrossRef]
8. O'Malley, R.; Glavin, M.; Jones, E. Vehicle detection at night based on tail-light detection. In *Proceedings of the 1st International Symposium on Vehicular Computing Systems*, Trinity College Dublin, Dublin, Ireland, 22–24 July 2008. [CrossRef]
9. Li, S.; Zhao, L. A Low-Cost and Fast Vehicle Detection Algorithm with a Monocular Camera for Adaptive Driving Beam Systems. *IEEE Access* **2021**, *9*, 26147–26155. [CrossRef]
10. O'Malley, R.; Glavin, M.; Jones, E. Vision-based detection and tracking of vehicles to the rear with perspective correction in low-light conditions. *IET Intell. Transp. Syst.* **2011**, *5*, 1–10. [CrossRef]
11. Gormer, S.; Muller, D.; Hold, S.; Meuter, M.; Kummer, A. Vehicle recognition and TTC estimation at night based on spotlight pairing. In *Proceedings of the 12th International IEEE Conference on Intelligent Transportation Systems*, St. Louis, MO, USA, 3–7 October 2009; pp. 196–201.

12. Tehrani, H.; Kawano, T.S. Car detection at night using latent filter. In Proceedings of the 2014 IEEE Intelligent Vehicles Symposium, Ypsilanti, MI, USA, 8–11 June 2014. [CrossRef]
13. Zeng, P.; Zhu, J.; Huang, G.; Cheng, L. Color Recognition of Vehicle Based on Low Light Enhancement and Pixel-wise Contextual Attention. In Proceedings of the 2020 2nd Symposium on Signal Processing Systems (SSPS 2020), Association for Computing Machinery, New York, NY, USA, 11 July 2020; pp. 13–17. [CrossRef]
14. Balci, B.; Elihos, A.; Turan, M.; Alkan, B.; Artan, Y. Front-View Vehicle Make and Model Recognition on Night-Time NIR Camera Images. In Proceedings of the 2019 16th IEEE International Conference on Advanced Video and Signal Based Surveillance (AVSS), Taipei, Taiwan, 18–21 September 2019; pp. 1–6. [CrossRef]
15. Götz, M.; Lee, M.H.; Han, Y.S.; Sung, Y.J. Sensor fusion for improvement of Adaptive high beam. *ATZ Worldw.* **2019**, *121*, 42–45. [CrossRef]
16. Gao, Z.; Li, Y. Control algorithm of Adaptive Front-lighting system based on Driver preview behavior. In Proceedings of the 2013 2nd International Conference on Measurement, Information and Control, Harbin, China, 16–18 August 2013. [CrossRef]
17. Bradai, B.; Herbin, A.; Ph Lauffenburger, J.; Basset, M. Predictive navigation-based virtual sensor for enhanced lighting. In Proceedings of the 7th International Symposium on Automotive Lighting (ISAL), Darmstadt, Germany, 25–26 September 2007; pp. 304–312.
18. Choi, H.; Lee, W.-S.; Harisha, B.S.; Kim, W.-C.; Lim, J. Optical Design for Laser Diode Scanner Headlamp with Efficiently Distributed Optical Power for Adaptive Driving Beam System of Automobiles. *Appl. Sci.* **2021**, *11*, 793. [CrossRef]
19. Synopsys. *LucidDrive Manual-LucidDrive Night Drive Simulation*. 2018. Available online: <https://www.synopsys.com/support.html> (accessed on 1 September 2021).
20. Synopsys. *RoadEditor Manual-LucidDrive Night Drive Simulation*. 2018. Available online: <https://www.synopsys.com/support.html> (accessed on 1 September 2021).
21. American Association of State Highway and Transportation Officials. Horizontal Alignment—Minimum Radius. In *A Policy on Geometric Design of Highways and Streets*; American Association of State Highway and Transportation Officials: Washington, DC, USA, 2001; p. 142.
22. National Highway Traffic Safety Administration (NHTSA); Department of Transportation (DOT). “Federal Motor Vehicle SAFETY Standards; Lamps, Reflective Devices, and Associated Equipment—A Proposed Rule by the National Highway Traffic Safety Administration on 10/12/2018.” Federal Register, 12 October 2018. Available online: <https://www.federalregister.gov/documents/2018/10/12/2018-21853/federal-motor-vehicle-safety-standards-lamps-reflective-devices-and-associated-equipment> (accessed on 1 September 2021).
23. American Association of State Highway and Transportation Officials. Horizontal Alignment—Design for Rural Highways, Urban Freeways, and High-Speed Urban Streets. In *A Policy on Geometric Design of Highways and Streets*; American Association of State Highway and Transportation Officials: Washington, DC, USA, 2001; pp. 143–145.
24. Mazzae, E.N.; Baldwin, G.H.S.; Andrella, A.; Smith, L.A. *Adaptive Driving Beam Headlighting System Glare Assessment*; National Highway Traffic Safety Administration: Washington, DC, USA, 2015; (Report No. DOT HS 812 174).
25. National Safety Council. Following Distance—Three-second following distance. In *Defensive Driving Courses—The DDC Instructor and Administrative Reference Guide*; National Safety Council: Chicago, IL, USA, 2005.
26. Society of Automotive Engineers. Adaptive Driving Beam. *SAE Int.* **2016**. [CrossRef]
27. Zadeh, L. Fuzzy sets. *Inf. Control.* **1965**, *8*, 338–353. [CrossRef]
28. MathWorks. Fuzzy Logic Toolbox: User’s Guide. Available online: <https://ww2.mathworks.cn/help/fuzzy/index.html> (accessed on 4 September 2021).